

000
001
002
003
004
005
006
007
008
009
010
011054
055
056
057
058
059
060
061
062
063
064
065
066
067
068
069
070
071
072
073
074
075
076
077
078
079
080
081
082
083
084
085
086
087
088
089
090
091
092
093
094
095
096
097
098
099
100
101
102
103
104
105
106
107

Partial Matching of 3D Shapes using Deformable Diversity

Anonymous CVPR submission

Paper ID ****

Abstract

We propose a novel approach for the matching of partial deformable shapes in 3D. Inspired by recent advances in 2D template matching techniques, our method relies on the concept of deformable diversity similarity(DDIS), extends and adapts it from an image to the 3D shape domain, and leverages the distinct behavior of this framework in different scales to achieve shape correspondences. We evaluate this framework on the SHREC16 partial matching of deformable shapes and show state of the art performance in achieving sparse correspondences. **AT: order of work:** **1. Section 3 (Approach), 2. Section 4 (Similarity), Section 5 (Results), Section 2 (Related work), Section 1 (Introduction).** Currently only Section 3 is sort of done

1. Introduction

Shape correspondence is a fundamental and challenging problem in computer vision and graphics. It has usage in various applications such as transferring texture and animation. Shapes rarely, if ever manifest in only one pose. While rigid transformations between surfaces is a well researched topic with many adequate solutions, a more challenging problem arises when a shape is deformed non-rigidly, a case all too common for people, animals and objects. Moreover, the shape acquisition process almost always lead to partiality of the scanned object. Occlusions arise from different angles of acquisition, which cause an object to occlude itself, or stem from other occluding objects. An additional type of difficulty which might be occur is topological noise, occurring when shapes touch pn another, thus making sensors unable to seperate them. All of these combined give rise to the challenging problem of partial correspondences, where a deformed and incomplete shape, possibly with topological changes, has to be matched with its full version. The goal of this paper is to deal with this challenging problem.

While in a rigid setting the problem can be solved by RANSAC and ICP like approaches[26, 11], extending these to non-rigid case produces mediocre results due to an un-

derlying assumption of small deformations. Early methods specialized for the non-rigid problem focused on minimization of intrinsic metric distortion[6, 36] and regularity of parts[?, 4]. These methods all contain with them a global assumption of isometry which holds only approximately, these tended to break down with it, and are also unable to handle extreme partiality. Another family of method is based on functional correspondence. These methods model correspondences as a linear operator of a known nature between a space of functions on manifolds[20]. These methods, originally designed for the full shape correspondence scenario have achieved state of the art results on various partial matching tasks in the recent years[16, 37, 24], and produce dense correspondence maps, but are not parallelizable, and their reliance on intrinsic metrics makes them invariant to symmetry.

We take a different approach. We take advantage of the fact that while the isometric property tends to break over large distances, it usually holds approximately in limited environments. These also tend to suffer a lot less from boundary effects, especially when concentrated around the extremities of a shape.

We can thus treat the problem of partial correspondences as matching of multiple templates, each smaller then the partial surface centered around shape landmarks.

In addition, since point descriptors are known to be modified by partiality and deformations, instead of using them directly, we follow the approach off[34](DDIS) which tackles template matching in 2D and use simple statistical assumptions on the nature of nearest neighbors between small patch descriptors, along with the assumption of an approximate conservation of distances in medium environments to obtain similarity scores between these partial shape templates.

We analyze the behavior of DDIS similarity in different scales and devise a multi scale scheme which leverages the advantages of each scale while masking their shortcomings.

We show that using this approach, we are able to generate a set of sparse correspondences, which are less prone to symmetrical assignment than functional correspondence reliant methods, and are of superior quality on the SHREC16

108 Partial matching challenge[8]. We then demonstrate how
109 these sparse correspondences can be used as an input to ex-
110 isting functional correspondence algorithms to obtain dense
111 correspondences or a higher quality. In summary, our con-
112 tributions are:
113

- 114 • A non trivial extension of Deformable Diversity from
115 2 to 3 Dimensions.
- 116 • A modified DDIS similarity measure which is more
117 well suited to handle matching of templates with a dif-
118 ferent number of points.
- 119 • An empirical analysis of DDIS behavior in different
120 scales, leading to an improved multi-scale framework.
- 121 • A multi-template approach to partial matching of de-
122 formable shapes which can both produce state of the
123 art sparse correspondences, and be used as an input
124 to functional correspondence algorithms, significantly
125 improving the results obtained by these.
126

127 The rest of the work is organized as follows: in section
128 2 we go over related works in the field of shape analysis.
129 Section 3 introduces our Deformable Diversity framework
130 for 3D shape matching. Experiments and results are given
131 in section 4, and the conclusions are in section 5.
132

133 2. Related work

134 2.1. Matching Of Deformable Surfaces

135 As a fundamental problem in computer graphics and vi-
136 sion, an extensive body of work have been done on the
137 matching of surfaces. A variety of shape descriptors have
138 been devised for this task which can be roughly divided in
139 to 2 families. Extrinsic ones, such as PFH[27], SHOT[35]
140 and FPFH[26] which are usually calculated in euclidean
141 space and are thus sensitive to non rigid deformations, but
142 can discern between reflections and are also more robust to
143 noise, topological artifacts and boundary effects. On the
144 other hand intrinsic features such as Heat[7] and Wave Ker-
145 nnel signatures[2] are invariant under isometric transfor-
146 mations, but are very sensitive to partiality and are unable to
147 discern between symmetric parts. These have been com-
148 monly used to generate rough correspondences between
149 surfaces and point clouds based on their similarity, but are
150 noisy and offer little in terms of bijectivity and continu-
151 ity of the solution. a measure of global consistency using
152 these can be achieved by solving an energy minimization
153 of the disimilarity matrices stemming from an assignment,
154 and the auction algorithm has been commonly employed
155 for this purpose. Other methods use pairwise relations be-
156 tween points such as geodesic distances[29, 30, 31], and
157 search for a configuration which minimizes the distor-
158 tions of these. These methods usually carry a high complexity,
159

160 both due to calculating the pairwise relations, and the com-
161 binatorial configuration search, and are thus either obtain
162 sparse matches[29, 30, 31] to alleviate this complexity, or
163 used strategies such as coarse to fine solutions. Another
164 common approach has been to embed the shapes into a dif-
165 ferent lower dimension "canonical" space, this has been
166 done by generalized MDS[6], an embedding into the mo-
167 bius group[15], or by representation in the LBO basis[32]
168 A notable family of works are derived from functional cor-
169 respondences. Introduced at[20, 22, 14, 37] these assume
170 that functions can be mapped from one manifold to an-
171 other via a linear operator, finding this transfer operator
172 allows to embed point in a space where the ICP method
173 can obtain correspondences. Lately there has been a large
174 body of works which employ learning methods such as Ran-
175 dom Forests[23] and deep learning architectures[17, 3, 19].
176 These show the promise of achieving state of the art per-
177 formance, but require a lot of annotated data.
178

179 2.2. Partial Matching of Deformable shapes

180 The introduction of partiality adds complications which
181 are not present in the full correspondence scenario. Spectral
182 quantities change drastically, while geodesic paths dis-
183 appear. For the rigid setup, the Iterative Closest Point(ICP)[1]
184 algorithm, preceded by initial alignment[28] tackle partial
185 matching successfully. Adapting this to the rigid setup how-
186 ever has proved to have limited success due to the alignment
187 which is necessary, and thus is only fit for very small non-
188 rigid deformation.
189

190 Early works which were designed with partial matching
191 in mind[4, 5] formulated an energy minimization prob-
192 lem over metric distortion and regularity of correspond-
193 ing parts. Following works relaxed the regularity require-
194 ment by allowing for sparse correspondences[36, 25]. Other
195 works[30, 29] minimized the distortion metric over the
196 shape extremities by doing combinatorial search of least
197 distortion matches and then densify them while employing
198 a refining scheme in the process.
199

200 In[21] a bag of words point-wise descriptors on a part in
201 conjunction with a constraint on area similarity and the reg-
202 ularity of the boundary length to produce correspondence
203 less matching parts without point to point correspondences
204 by energy minimization.
205

206 Another line of works employ machine learning tech-
207 niques to learn correspondences between manifolds. Re-
208 cently [24] had proven that partiality induces a slanted di-
209 agonal structure in the correspondence matrix and found
210 the Laplacian eigenfunctions from each basis which induces
211 this structure. Current state of the art[16] uses this notion in
212 conjunction with joint diagonalization. The main drawback
213 of this method, shared with other intrinsic methods, is its
214 invariance to symmetries.
215

216 3D Shape Descriptors

216
217
218
219
220
221
222
223
224

2.3. Template matching in 2D

Template matching in 2D is a well researched topic. Similarly to 3D objects are going complex deformations of pose, and are only seen partially depending on the camera point of view. Recently a series of works which use a very simplistic framework based on the statistical properties of nearest neighbors in low level feature space had made good strides in tackling this complex task.

Best Buddies Similarity Great strides had been achieved in the field of 2D template matching. Best Buddies Similarity[9] is a simple framework which employs a statistical assumption - if two regions \mathcal{N}, \mathcal{M} contain the same template patches should maintain Bi Directional Similarity. That is - given a point $n_i \in \mathcal{N}$ and a corresponding point $m_i \in \mathcal{M}$ they should point to each other as nearest neighbors - that is if $NN_{\mathcal{M}}(n_i) = m_j$ then on a matching template we should expect $NN_{\mathcal{N}}(m_j) = n_i$. Solving for a matching template then amounts to finding the region which has the highest count of best buddies. This amazingly simple scheme has been shown to be able to handle occlusions, missing parts and complex deformations of templates.

Deformable Diversity Similarity Building upon the above work, [34] relaxed the requirement for a best buddy relation, and added a requirement for spatial coherency.

The rather cumbersome best buddy relation has been relaxed to requiring only that the diversity of the set of nearest neighbors sets between corresponding templates should be high. This is actually prerequisite to a high best buddies similarity score and serves as a rough approximation of it. For this end diversity is formally defined as:

$$DIS = c \cdot |\{n_i \in \mathcal{N} : \exists m_j \in \mathcal{M}, NN(m_j, \mathcal{N}) = n_i\}| \quad (1)$$

where $|\cdot|$ denotes group size and $c = 1/\min(|\mathcal{M}|, |\mathcal{N}|)$ is a normalization factor. Between non corresponding windows, indeed one should expect most points to have no real corresponding point, and thus be mapped to a very and remote nearest neighbors. On the other hand, regions containing matching objects are drawn from the same distribution, thus the diversity of nearest neighbors should be high. To accommodate this assumption not only did they rewarded high diversity of nearest neighbors, but also penalized mapping to the same patch. To this end, another, a negative diversity measure had been defined:

$$\kappa_{\mathcal{M}}(n_i) = |\{m \in \mathcal{M} : NN^a(m, \mathcal{N}) = n_i\}| \quad (2)$$

With x_i^a denoting the appearance descriptor of point x_i . Thus the contribution of a patch $m_j : NN^a(m_j, \mathcal{N}) = n_i$ is $\exp(1 - \kappa_{\mathcal{M}}(n_i))$. An additional observation made has been that while non isometric deformations do occur, they should be restricted, small, in real objects. With distance on the window pixel grid between 2 nearest neighbor points

defined as $r_j = d(m_j^l, n_i^l)$ with x_i^l denoting the location of x_i on a grid, the final Deformable Diversity Similarity formulation becomes:

$$DDIS = c \sum_{\mathcal{N} \rightarrow \mathcal{M}} \frac{1}{1 + r_j} \cdot \exp(1 - \kappa(NN^a(m_j, \mathcal{N}))) \quad (3)$$

3. General Approach

Given two surfaces \mathcal{M} and \mathcal{N} , the goal is to find the best match of \mathcal{N} within \mathcal{M} . In particular, we aim at extracting a sparse set of point correspondences between the models. Our approach is based on three key ideas, which we describe hereafter.

First, inspired by [34], similarity is captured by two properties of the Nearest Neighbor field. (1) When \mathcal{N} and a patch of \mathcal{M} match, most points in \mathcal{M} have a unique NN-match in \mathcal{N} . This implies that the NN field should be highly diverse, in the sense that many different points in \mathcal{N} are being matched. (2) Arbitrary matches typically imply a large deformation, whereas correct matches should preserve the distance between pair of points. Therefore, Similarity should be based both on the diversity of the Nearest-Neighbor field and on the consistency of the distances between the points.

Second, rather than realizing the similarity test, described above, on \mathcal{N} as a whole, it is preferable to perform it on a set of small sub-surfaces of \mathcal{N} . This is so not only since a small sub-surfaces is more likely to exhibit consistent distances, but also since it is less likely to be matched to a repeating pattern, which would lead to smaller diversity.

Third, a multi-scale approach with respect to the size of matched sub-surfaces is beneficial. This is so since larger surfaces contain more global context, resulting in matches which lie in a correct region, but provide poor localization. On the other hand, matching smaller surfaces lead to results which are better locally, but may be globally inconsistent.
AT: what do you mean by globally inconsistent?

Therefore, our algorithm, which is illustrated in Figure 1, consists of the following steps.

1. **Pre-processing.** Shape descriptors are calculated for every vertex of both meshes and an approximate nearest neighbor field is computed for the vertices, as described hereafter.

Many descriptors have been proposed in the literature [28, 35, 33]. We use the FPFH [26], which is robust to small deformations and partiality of the data, yet sensitive to symmetrical flips. **AT: what makes it sensitive to symmetrical flips?** Therefore, it addresses a major drawback of matching a right arm, for example, to the left one. We then compute a nearest neighbor field mapping, by assigning each vertex of \mathcal{M} its nearest neighbor in \mathcal{N} , FPFH-wise.

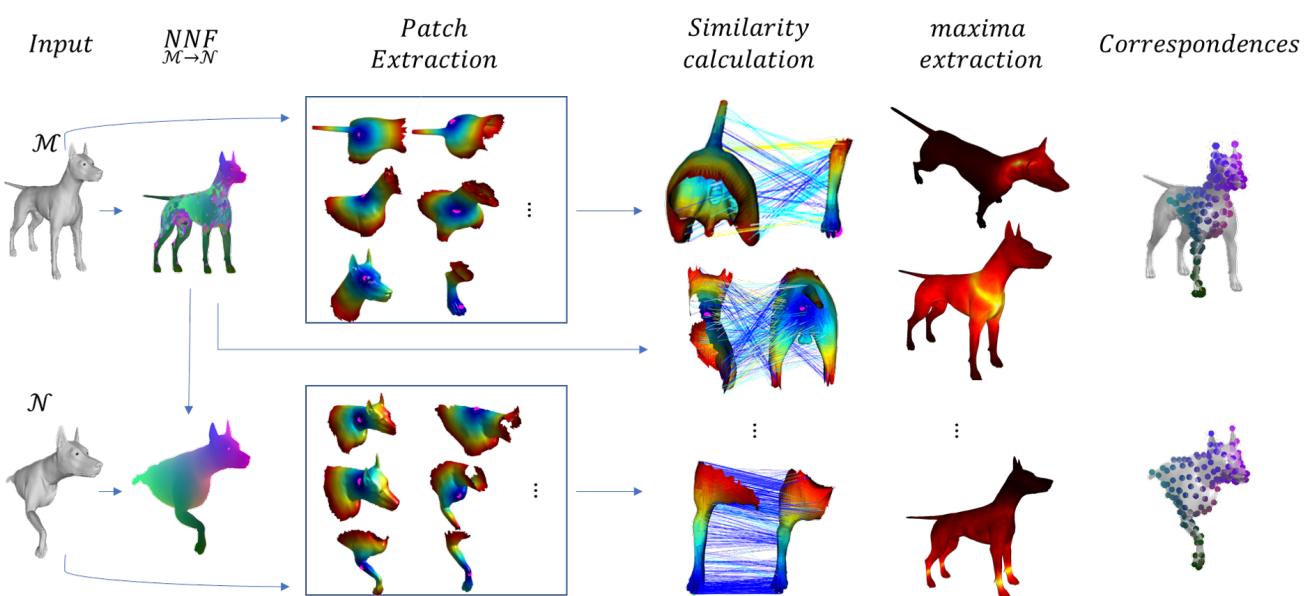


Figure 1. **Algorithm outline.** In the first step, we compute the nearest-neighbor field for \mathcal{N} and \mathcal{N} . Then, patches of the surfaces are extracted for every sample point in \mathcal{N} and for every vertex on \mathcal{M} . These patches cover the surface (i.e., may overlap) and represent semantic regions. Note that exact segmentation is not needed. Step 3 is the core of the algorithm, in which the similarity between the patches is computed. Finally, in Step 4, for every sample of \mathcal{N} we set the vertex of \mathcal{M} that achieves the maximal score as its corresponding point. **AT: This figure should be re-done**

2. Patch extraction. Inline with the second key idea, we aim at extracting a meaningful set of sub-surfaces, which cover (rather than partition) the surface. This is done in two steps: First, we extract a meaningful set of points, whose neighborhoods provide a good cover of the surface. We then extract the patches using this sample. We elaborate hereafter.

To extract the sample point set, we start from the extremities of the surface, which are considered salient points. A vertex is considered to be an extremity if it resides on a tip of the surface (e.g., tips of limbs) [12]. In practice, we define them to be vertices that are local maxima of the sum of the geodesic distance functional. Formally, $\forall v \in S$, let N_v be the set of neighboring vertices of vertex v . Let $GeodDist(v_i, v_j)$ be the geodesic distance between vertices v_i and v_j of mesh S . Vertex v is an extremity if it satisfies

$$\sum_{v_i \in S} GeodDist(v, v_i) > \sum_{v_n \in S} GeodDist(v_n, v_i). \quad (4)$$

Then, we iteratively add more samples, choosing the next sample point as follows. We construct a "forbidden" region around every point in the set. This region is a geodesic disc of radius $0.05\sqrt{\text{Area}(\mathcal{M})}$. The next point to be added to the set is a vertex whose geodesic distance to any sample point in the set is minimal and does not fall in any of the forbidden regions. This pro-

cess stops when the entire surface is marked forbidden.

Once the set of representing sample set is defined, a disc (sub-surface) of geodesic distance R_T is extracted around each sample point, which is the sought-after set of patches. Specifically, $R_T = \beta \cdot \sqrt{\text{Area}(\mathcal{M})}$. As our approach is multiscale, β , which was found empirically by minimizing the error of correspondences on a training set, varies. In practice we use $\beta = \{0.6, 0.4, 0.2\}$.

3. Computing similarities between pairs of patches.

This step is the core of our algorithm, which realizes the first key idea.

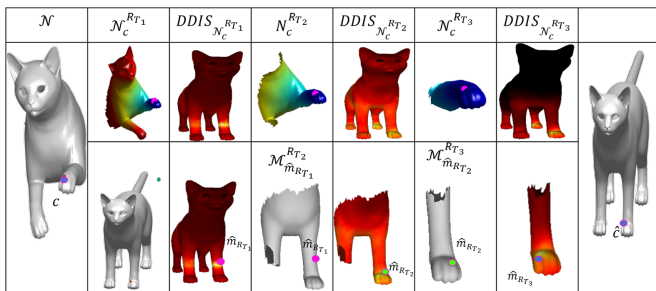
For each pair of patches of the same scale, $Q_i \subset \mathcal{M}$ and $P_i \subset \mathcal{N}$, we compute a similarity value. Recall that our goal is to reward a nearest-neighbor field with high diversity and low deformation. We will define the similarity function $DDIS$ that achieves it in Section 4. This is done in a multi-scale manner.

4. Extracting a sparse set of corresponding points.

Given the similarity values between the patches, our goal now is to extract a set of corresponding points between \mathcal{N} to \mathcal{M} . If we had a single scale, then for each sample point (the center of a patch) of \mathcal{N} , we would choose the vertex of \mathcal{M} that maximizes the similarity function.

In our multi-scale approach, we proceed from coarse

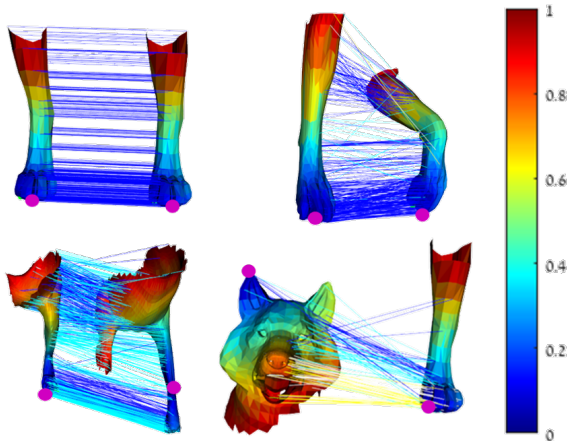
432 to fine. Suppose that $P_i \subset \mathcal{N}$ and $Q_j \subset \mathcal{M}$ were
 433 found to have the highest similarity in a coarsest scale
 434 (i.e. Q_j is the largest). The coarsest match is then
 435 set between $v_i \in P_i$ and $w_j \in Q_j$, where v_i, w_j are
 436 the *geodesic centers* of P_i, Q_j , respectively (i.e. the
 437 sample points that define the patches in Step 2). When
 438 moving to the finer scale, we replace Q_j with a smaller
 439 (finer) patch in which w_j is the center and set the new
 440 w_j to be the vertex on this patch that maximizes the
 441 similarity function $DDIS$ on this patch. The finest w_j
 442 is the corresponding point of v_i ; see Figure 2.
 443



444
 445
 446
 447
 448
 449
 450
 451
 452
 453
 454
 455
 456
 457
 458
 459
 460
 461
 462
 463
 464
 465
 466
 467
 468
 469
 470
 471
 472
 473
 474
 475
 476
 477
 478
 479
 480
 481
 482
 483
 484
 485
Figure 2. Multi-scale similarity. Given the sample point on the left (in magenta), the corresponding points on \mathcal{M} are shown on the right. In the coarsest level, the general region of the matching point is found, but the point is imprecise. In subsequent levels, the general region is not found. Our multi-scale approach manages to find the precise point. **AT: Replace the image.**

462
 463
 464
 465
 466
 467
 468
 469
 470
 471
 472
 473
 474
 475
 476
 477
 478
 479
 480
 481
 482
 483
 484
 485
5. Coherency-based Post processing AT: I do not understand what you do and why. As always: first sentence- goal of the step and why it is needed. second sentence - key idea of how to do that. the rest of the sentences - explanation of how you do that WITHOUT unnecessary mathematical notations. Rewrite **NA: proposed text:** Given the set of sparse correspondences obtained in step 4, in the last step we aim at identifying incorrect ones and replace them with more fit correspondences. We first detect ill fitted Correspondences. Assuming most of our correspondence from step 4 are correct ones, bad matches would have to be outliers. We use the deformation(deviation of distance between other corresponding pairs) as a way to detect these. We calculate for each pair, the mean of distance differences between other correspondences. We then mark correspondences whose mean distance difference to other correspondences is larger by more than 15% then the mean distance difference. For each such suspect correspondence, we employ a greedy search for a local maxima of $DDIS$ which minimizes the deformation w.r.t. good correspondences and set it as the final correspondence.

4. Similarity



486
 487
 488
 489
 490
 491
 492
 493
 494
 495
 496
 497
 498
 499
 500
 501
 502
 503
 504
 505
 506
 507
 508
 509
 510
 511
 512
 513
 514
 515
 516
 517
 518
 519
 520
 521
 522
 523
 524
 525
 526
 527
 528
 529
 530
 531
 532
 533
 534
 535
 536
 537
 538
 539
Figure 3. Nearest Neighbor Field. The surfaces are colored by the geodesic distances from the magenta point; the lines are colored by the **NA: difference of geodesic distances from the purple point.** **AT: deviation of what?** Clearly, similar surfaces on the top (even when deformed) exhibit diversity in matching (i.e. different points on one surface are matched to different points on the other). Furthermore, in this case, most lines are blue, which indicates similar distances from the source point. This is not the case at the bottom, where the surfaces are highly different from one another.

Given a target \mathcal{M} and \mathcal{N} (Section 3) and a vertex $v \in \mathcal{N}$ **AT: yes?, not the opposite?**, the goal is to find the most similar vertex on \mathcal{M} . We would like the similarity to be oblivious to non-rigid transformation, to the resolutions of the meshes, to noise, and to the partiality of the data.

NA: proposed rewrite: We would like to measure the similarity between two surface patches, a target patch \mathcal{Q} and a template patch \mathcal{P} , defined by geodesic discs of a radius R_T around the points c' and c respectively. We would like the similarity to be oblivious to non-rigid transformation, the resolutions of the meshes, noise, and partiality of the data. **AT:**

Second paragraph: Key idea, first in laymen language. We are inspired by..., but found that the method there is insufficient due to the following reasons.

Third paragraph: the mathematical definition that realizes the key idea

Fourth paragraph: outline of similarity computation

Then, paragraphs/subsections explaining the different stages

NA: Second paragraph: Key idea, first in laymen language. proposed text:

We are inspired by the principles introduced in[34]: the idea that the similarity between the target and the template is captured by two properties of the nearest neighbor field between points of a target and a template

540
 541 patch. The first is that the diversity of NN matches forms
 542 a strong cue for template matching. The second key idea
 543 is to explicitly consider the deformation implied by the
 544 nearest neighbor field by rewarding the preservation of
 545 distances.

546 The movement from 2 to 3 dimensions introduces an
 547 additional challenge addressed by our modified similarity
 548 measure.

549 The geodesic disc which is the simple replacement for
 550 a search window introduces a couple of problems.

551 Chief of which is an inequality between both the area
 552 and number of points between the target and the patch.
 553 Especially in the partial setup, the geodesic disc on the
 554 target will commonly be of an area which is bigger or
 555 equal to that of the template. This leads to the inclusion
 556 of repeating patterns or symmetrical parts which affect
 557 the diversity of the Nearest neighbor field.

558 This suggests that while we should still expect a diverse
 559 nearest neighbor field, correct matches have a higher
 560 probability to share a nearest neighbor with an
 561 incorrect one. Thus our similarity measure should not
 562 penalize a shared nearest neighbor. Instead we should
 563 count only the match whose implied deformation is the
 564 lowest.

565 NA: Third paragraph: the mathematical definition
 566 that realizes the key idea, proposed text:

567 Given a target candidate patch $\mathcal{M}_{c'}^{R_T}$ and a tem-
 568 plate patch $\mathcal{N}_c^{R_T}$, defined by a geodesic disc of ra-
 569 dius R_T around the vertex $c' \in \mathcal{M}$ and $c \in \mathcal{N}$
 570 respectively, a nearest neighbor field mapping each
 571 vertex on \mathcal{M} to its nearest neighbor on \mathcal{N} in some
 572 shape descriptor space, and the geodesic distances
 573 $\{g(c', m_j)\}_{m_j \in \mathcal{M}_{c'}^{R_T}}, \{g(c, n_i)\}_{n_i \in \mathcal{N}_c^{R_T}}$, the similarity of
 574 $\mathcal{M}_{c'}^{R_T}$ to $\mathcal{N}_c^{R_T}$ is calculated by Eq. 5:

$$DDIS_{\mathcal{N}_c^{R_T}}(\mathcal{M}_{c'}^{R_T}, \gamma) = \sum_{n_i \in \mathcal{N}_c^{R_T}} \frac{1}{1 + r_i} \quad (5)$$

575
 576 NA: Where r_i is the deformation implied by the NNF
 577 for n_i as defined by Eq. 6

$$r_i = \begin{cases} \min_{NN(m_j, \mathcal{N})=n_i} \frac{|g(m_j, c') - g(n_i, c)|}{\gamma \cdot R_{\mathcal{M}}} & m_j \in \mathcal{M}_{c'}^{R_T} \\ \infty, & \text{else} \end{cases} \quad (6)$$

578 where $\gamma \cdot R_{\mathcal{M}}$ is a regularizer on the error length and
 579 should ideally be set according to the expected distor-
 580 tion. We notice the case where $r_i \in \{0, \infty\} \forall n_i$. When
 581 this occurs $1/r_i \in \{1, 0\}$ and DDIS counts the number
 582 of points in \mathcal{Q} which are a NN of any point in \mathcal{P} . This is
 583 exactly the diversity of the NN field.

584 NA: Fourth paragraph: outline of similarity compu-
 585 tation: proposed text:

594 To calculate our similarity we first compute shape de-
 595 scriptors for all the points on \mathcal{N}, \mathcal{M} and use Approx-
 596 imate NN in descriptor space to infer the Nearest Neigh-
 597 bor Field. We then collect a neighborhood $\mathcal{N}_c^{R_T}$ of a
 598 given Radius R_T around a desired source point n_c and
 599 compute the distance of all points which lie within this
 600 neighborhood to the source n_c . We repeat the same pro-
 601 cess for a candidate point $m_c \in \mathcal{M}$ to create $\mathcal{M}_c^{R_T}$. We
 602 traverse all the points in $\mathcal{M}_c^{R_T}$ and check for each one
 603 if it's distance to its center is the most similar to the dis-
 604 tance of its nearest neighbor in $\mathcal{N}_c^{R_T}$ and update r_i ac-
 605 cordingly. Finally we use

606 NA: subsections explaining the different stages, pro-
 607 posed text:

4.1. Shapes Preprocessing

608 Before we can calculate similarity between our shapes
 609 some preprocessing of the shapes is necessary. We calcu-
 610 late a characteristic length on the full part denoted
 611 $R_{\mathcal{M}} = \sqrt{\text{Area}(\mathcal{M})}$. We also compute vertex-wise nor-
 612 mals using the face normal weighting scheme introduced
 613 in[18].

4.2. Nearest Neighbor Field calculation

614 To infer our nearest neighbor field we first calculate
 615 FPFH[26] point descriptors for every point on the tem-
 616 plate \mathcal{N} and the query shape \mathcal{M} . We set a neighborhood
 617 of $r_F = \alpha \cdot R_{\mathcal{M}}$ and around every point, where α is a
 618 tunable parameter for the calculation of FPFH. We then
 619 calculate approximate nearest neighbors in FPFH space
 620 using FLANN with a χ^2 distance measure to obtain a
 621 nearest neighbor mapping $NNF = \{NN(m_i, \mathcal{N})\}_{i=1}^{|\mathcal{M}|}$

4.3. Template construction

622 In order to calculate our similarity measure, another
 623 necessary step is to have 2 pieces of roughly the same
 624 volume, and a way to compare the locations of points
 625 on them. In the absence of a simple grid, this is done
 626 by picking a reference point x as the center and collect-
 627 ing all the points in a surrounding neighborhood of a
 628 defined radius $R_T = \beta R_{\mathcal{M}}$, where beta is a tunable pa-
 629 rameter. We calculate the distance from the reference
 630 point to every point on the selected piece. This is done
 631 once for a chosen point $n_c \in \mathcal{N}$ to construct $\mathcal{N}_c^{R_T}$.

4.4. Similarity Calculation

632 We iterate over all points $m_{c'} \in \mathcal{M}$ and construct
 633 $\mathcal{M}_{c'}^{R_T}$. Inside the piece we iterate over every point $m_j \in$
 634 $\mathcal{M}_{c'}^{R_T}$ and calculate $r_i = \frac{|(d(m_i^l, m_{c'}^l) - (NN(m_i, \mathcal{N})^l, n_i^l))|}{\gamma \cdot R_{\mathcal{M}}}$,
 635 where if $NN(m_j, \mathcal{N})$ is outside $\mathcal{N}_c^{R_T}$ this distance is dis-
 636 regarded. Notice the normalization by $\gamma R_{\mathcal{M}}$ here which
 637 is done to make the distances scale invariant, while γ is
 638 639

648
 649
 650
 651
 652
 653
 654
 655
 656
 657
 a tunable parameter which should correlate to the expected distortion. We find for each $n_i \in \mathcal{N}_c^{R_T}$ the distance of the point who is pointing to it as a nearest neighbor and has the most similar distance to its reference point. If n_i has no point who point to it as its nearest neighbor then $r_i = \infty$. Finally we calculate The similarity between the pieces by our similarity function in Eq. XX.

5. Deformable Diversity Similarity in 3D

659
 660
 661
 662
 663
 664
 665
 666
 667
 668
 669
 670
 671
 672
 673
 674
 675
 676
 677
 NA: Old text: The nature of 3D data gives rise to unique problems which do not occur in the 2D scenario. Data is distributed in space both sparsely and with varying densities - the amount of data points occupying a given volume can vary drastically. A second problem arises from the absence of a regular grid. These problems require different definitions for key components to the 2D deformable diversity formulation. For this work we chose the image patch to be replaced by a neighborhood which is required to calculate a selected shape descriptor, usually a small sphere in euclidean space or a surface patch with a radius r_F . The search window of a template is defined as a geodesic disc around the query point, with a radius denoted by R_T . The pixel grid distance is replaced by either a euclidean distance $d_{Euc}(x^l, y^l)$ (in the case of point clouds) or geodesic distance $d_{Geo}(x^l, y^l)$ (for surface meshes). Given these DDIS between shape parts \mathcal{M}_{x,R_T} and \mathcal{N}_{y,R_T} can be naively formulated as:

$$678 \quad DDIS = c \cdot \sum_{m_j \in \mathcal{M}_{x,R_T}} \frac{\exp(1 - \kappa(NN^S(m_j, \mathcal{N}_{y,R_T})))}{1 + r_j} \quad (7)$$

682 where \mathcal{M}_{x,R_T} and \mathcal{N}_{y,R_T} are the shape parts in a radius R_T surrounding the points $x \in \mathcal{M}$ and $y \in \mathcal{N}$ respectively, r_j is the induced deformation

$$686 \quad r_j = \frac{|d(m_j^l, m_x^l) - d(NN^S(m_j, \mathcal{N}_{y,R_T})^l, n_y^l)|}{\gamma \cdot R_T} \quad (8)$$

689 where γ is a selected fraction and c is a normalization coefficient $c = 1/\min|\mathcal{N}_{y,R_T}|, |\mathcal{M}_{x,R_T}|$.

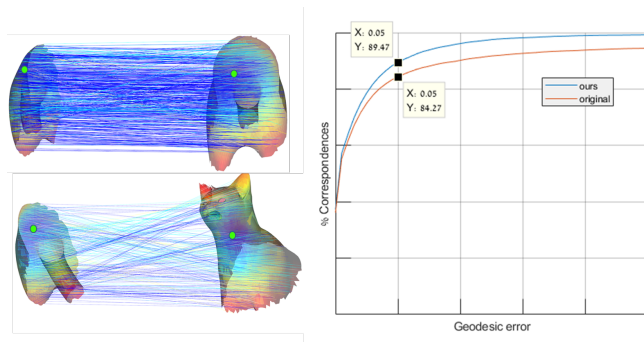
690 However, we wouldn't like to penalize our similarity score in case of repeating patterns or symmetrical shapes which have both symmetries in the template search window. Intuitively and empirically the exponent is too harsh and indeed unnecessary as both deformity and diversity will attenuate the score in case of multiple nearest neighbors. On the other hand, we wouldn't want to reward far correspondences at all because they are unlikely to originate from a corresponding patch.

700 To account for this the following formulation has been found to work better: given a point $n_i \subset \mathcal{N}_{y,R_T}$ has a set

702
 703
 704
 705
 706
 707
 708
 709
 710
 711
 of nearest neighbors in descriptor space on a geodesic disc $\mathcal{M}_{n_i} = \{m_j \in \mathcal{M}_{j,R_T} : NN^S(m_j, N_{y,R_T}) = n_i\}$, we define $m'_i = \operatorname{argmin}_{m_j \in \mathcal{M}_{n_i}}(r_j)$ and r'_i the minimal distortion distance, we add only the contribution of this point to the similarity score which then becomes

$$712 \quad DDIS(N_{y,R_T}, \mathcal{M}_{x,R_T}, \gamma) = \sum_{m'_i} \frac{1}{1 + r'_i} \quad (9)$$

713
 714
 715
 716
 717
 718
 719
 720
 721
 722
 723
 724
 725
 726
 explain why – can we see it visually on the same example? added both qualitative(visual, and quantitative example This equation still promotes both diversity and low defor-



727
 728
 729
 730
 731
 732
 733
 734
 735
 736
 737
 738
 739
 740
 741
 742
 743
 744
 745
 Figure 4. Qualitative and quantitative illustration of the improvement introduced by our formulation. On the top left the Nearest neighbor mapping between the part and its corresponding ground truth geodesic disc. As can be seen low distortion is occurring between the true corresponding points, but the symmetrical part which is not included on the partial model maps to the same points - thus attenuating the score originating from these. One the bottom left we see the piece chosen by the original DDIS formulation. The arrows with low distortion seldom have other points which are their nearest neighbors and thus achieves a better score without our modification. The cumulative error curves show an improvement of 5 percent on the training set using our formulation.

746
 747
 748
 749
 750
 751
 752
 753
 754
 755
 mations, but is less biased against surfaces which are either symmetrical, or exhibit repeating patterns and achieves a considerable improvement over the original formulation, as can be seen in Fig. XX.

5.1. DDIS Template Matching

746
 747
 748
 749
 750
 751
 752
 753
 754
 755
 Goal of the algorithm In this section we go over the flow of template matching of 3D shapes using DDIS, the solution of which constitutes the core of our partial shape matching. Given a template \mathcal{N}_{y,R_T} with a reference point n_y as it's center and a maximal distance R_T , we aim to find on a model \mathcal{M} which has a deformed version of it, the corresponding surface piece \mathcal{M}_{y^*,R_T} and it's center m_{y^*} . The solution is obtained by finding the point on \mathcal{M} whose surrounding geodesic disc maximizes the above mentioned DDIS measure. key ideas

756 Overview We'll first give an overview, and then give an
757 extended description of each of each stage.
758

We start by calculating the normals for \mathcal{M} and \mathcal{N} . We
759 than calculate local point descriptors for each patch of some
760 neighborhood around the points in each mesh(For our
761 purpose FPFH seemed to work the best of our tested de-
762 scriptors). Having calculated these, we calculate a nearest neig-
763 bor field by finding for each patch in \mathcal{M} it's Nearest Neig-
764 bor in \mathcal{N} . We now find the distance of every point $n \in \mathcal{N}$
765 to the desired point $y \in \mathcal{N}$ for a desired neighborhood R_T .
766 We now go over every point $x \in \mathcal{M}$. For each
767 we extract the geodesic disc \mathcal{M}_{x,R_T} around it. We take
768 notice that while the above stages are done here in the con-
769 text of template matching for one template, when matching
770 multiple templates all of the above calculations have to be
771 done only once between the shapes, with the exception of
772 geodesic distance field extraction for the template itself. Fi-
773 nally we calculate DDIS for this disc with $\mathcal{N}_{y,R}$ which has
774 y as it's center. Having done that for every point, the point
775 $y^* \in \mathcal{M}$ which gets the maximal DDIS Score is deemed
776 the corresponding point to y .
777

778 Point Normal Estimation There are various schemes
779 for estimating point normals given a triangulated mesh sur-
780 face. We have picked the one which is available in the stan-
781 dard PCL. Given a vertex p_i on a triangulated mesh \mathcal{X} and
782 it's associated polygons $\{A_j\}_{j=1}^k$ and their normals N_{A_j} the
783 point normal $N_i = \sum_{j=1}^k |A_j| \cdot N_{A_j}$

784 Local Patch Descriptor DDIS as defined by [34] uses
785 patch descriptors as low level features for their similarity
786 measure. While a patch in an image can be defined by
787 the images grid no such grid exists on 3D point clouds and
788 meshes, where density of data points can vary. Thus a patch
789 has to be defined by some geometric measure. While the
790 more robust way to define it would be using geodesic dis-
791 tance, since we are talking a small environment around a
792 point on the mesh we have found that for practical pur-
793 poses a patch in a defined euclidean radius r_F around a
794 point serves well enough. We pick this radius in the fol-
795 lowing way: given the full surface mesh \mathcal{M} we find it's
796 equivalent of a diameter $D_{\mathcal{M}} = \sqrt{\text{Area}(\mathcal{M})}$, and tune a
797 parameter α to obtain $r_F = \frac{\alpha}{*} D_{\mathcal{M}}$ A lot of local shape
798 descriptors have been used successfully in 3D shape anal-
799 ysis. We have tested the following descriptors: PFH[27]
800 SHOT[35],HKS[33],SIHKS[7],ROPS[10] and FPFH[26].
801 Out of these FPFH has achieved the best performance, and
802 thus the descriptor for the local patch has been chosen to be
803 FPFH.
804

805 Nearest Neighbor Field As an intermediate stage
806 towards the calculation of Deformable Diversity Simi-
807 larity measure, the calculation of the nearest neighbor
808 field(will be abbreviated as NNF) needs to be calcu-
809 lated. Thus for every patch $m \in \mathcal{M}$ we have to
 find the patch on the template $n \in \mathcal{N}$ which resem-

bles it the most. For $FPFH$, $NN^S(m_j, \mathcal{N})$ is defined
 $NN^S(m_j, \mathcal{N}) \equiv \underset{i}{\operatorname{argmin}} \chi^2(FPFH(m_j), FPFH(n_i))$
 and the Nearest Neighbor Field is the set of all these cor-
 respondences.

DDIS calculation For every point in $m_x \in \mathcal{M}$ we then
 extract a geodesic disk $\mathcal{M}_{x,R}$ with a radius R_T around it
 and calculate deformable diversity score for it. The point
 which maximizes the similarity score gives us a correspon-
 dence $(y, y^*) \in \mathcal{N} \times \mathcal{M}$.

5.2. DDIS Sparse Correspondences

A key takeaway from experimenting with DDIS as a
 template matching algorithm for partial matching has been
 that isometry does not hold, at least not globally. It does
 however, hold pretty well locally, especially at extremities.
 To this end we devise multiple template matching frame-
 work for Partial correspondences of deformable shapes. We
 first obtain landmarks $F_{init} = \{f\}_i$ as described in[]. We
 then employ a simple sampling scheme which ensures a
 good quasi uniform covering of the surface. Finally, we
 for each sample point we extract a geodesic disc, and find
 its counterpart on \mathcal{M} which maximizes DDIS.

Landmark Extraction We follow the work of[12] to ob-
 tain mesh extremities. Given a shape the work employs the
 following framework to extract it's extremities. A point is
 detected as an extremity if it fulfills 2 conditions: - it's sum
 of geodesic distances is a local extrema, formally, for $v \in S$
 , where S is a surface mesh, we define the set of points with
 a direct edge to it as N_v , the point is a critical point if :

$$\sum_{v_i \in S} d_{geo}(v, v_i) > \sum_{v_i \in S} d_{geo}(v_n, v_i), \forall v_n \in N_v \quad (10)$$

An additional requirement for it to be an extremities is for
 it to lie on the convex hull of the shape's MDS. In this work
 we have dropped the last condition, but chose N_{v^*} - a neigh-
 borhood of $0.03 \cdot \sqrt{\text{Area}(S)}$. This stage gives us the initial
 set of sample denoted S_0

Mesh sampling We employ a sampling scheme very
 reminiscent of the one employed in[31]. In each stage k ,
 we take the set of samples S_{k-1} and mark all the points in a
 radius R_S around them. From the set of remaining point we
 choose the one whose distance to the set S_{k-1} is minimal to
 create the set S_k . We repeat this process until all the points
 are marked.

Landmark Template Matching For this end, we cre-
 ate a template for each landmark point - we collect all sur-
 face point in a surrounding geodesic disc of radius $R_T =$
 $\beta \cdot \sqrt{\text{area}(\mathcal{M})}$. While it might seem natural to calculate a
 different nearest neighbor field for each landmark template
 it has been empirically found that using the global nearest
 neighbor field gives much better results. This is hypothe-
 sized to occur due to the fact that this nearest neighbor

810
 811
 812
 813
 814
 815
 816
 817
 818
 819
 820
 821
 822
 823
 824
 825
 826
 827
 828
 829
 830
 831
 832
 833
 834
 835
 836
 837
 838
 839
 840
 841
 842
 843
 844
 845
 846
 847
 848
 849
 850
 851
 852
 853
 854
 855
 856
 857
 858
 859
 860
 861
 862
 863

Algorithm 1 3DIS Sparse Correspondences

procedure DDIS CORRESPONDENCE($\mathcal{M}, \mathcal{N}, \alpha, \beta, \gamma$)
 Returns point correspondence for critical points on \mathcal{N}

$r_F \leftarrow \alpha / 100 \cdot \sqrt{\text{Area}(\mathcal{M})}$

$R_{\text{thresh}} \leftarrow \beta / 100 \cdot \sqrt{\text{Area}(\mathcal{M})}$

$N_{\mathcal{M}} \leftarrow \text{ComputeNormals}(\mathcal{M})$

$N_{\mathcal{N}} \leftarrow \text{ComputeNormals}(\mathcal{N})$

$F_{\mathcal{M}} \leftarrow \text{FPFH}(\mathcal{M}, N_{\mathcal{M}}, r_F)$

$F_{\mathcal{N}} \leftarrow \text{FPFH}(\mathcal{N}, N_{\mathcal{N}}, r_F)$

$NNF_{\mathcal{M} \rightarrow \mathcal{N}} \leftarrow \text{ANN}(F_{\mathcal{M}}, F_{\mathcal{N}})$

$\begin{array}{lcl} N_c & = & \{n : \sum_{n_i \in \mathcal{N}} d_{\text{geo}}(n, n_i) > \\ & & \sum_{n_i \in \mathcal{N}} d_{\text{geo}}(n_N, n_i), \forall n_N : d_{\text{geo}}(n, n_N) < \\ & & 0.03 \cdot \sqrt{\text{Area}(\mathcal{M})}\} \end{array}$

for $n_y \in N_c$ **do** ▷ DDIS calculation Loop

$m_{c*} \leftarrow \text{DDIS_Correspondence}(\mathcal{M}, n_y, \mathcal{N}, \alpha,$

end for

return $\mathcal{M}_c \times N_c = \{m_{c*}, n_c\}$

end procedure

field encodes global information when obtained this way and might eliminate local distractors.

Each landmark template is compared to all surface parts of a similar R_T on \mathcal{M} to obtain correspondences.

5.3. Cascaded Multi-Scale DDIS

The observation of the effects of the choice of β and the trade-off between finer localization and avoidance of global errors naturally leads to the adoption of a multi scale framework. We calculate *DDIS* score for multiple *beta* values, and use the location obtained with a large beta to select a narrow environment in which we look for the maximum of DDIS with a smaller value *beta*, thus using the larger scale to get a rough global location, and the smaller scale to fit it into a more exact location. While this might be done at multiple custom scales we have found that the triplet $\beta, 2 \cdot \beta/3, \beta/3$ works well.

5.4. Greedy Outlier Fix

The results obtained by the pipeline, while empirically already producing matches of superior quality to state of the art algorithms in the field nevertheless have no explicit requirement on generating a coherent set of matches. We thus as a post processing step identify outliers and replace them with more suitable correspondences. Inspired by distortion minimization methods such as[31] we pick the distortion of a correspondence as a measure of its coherency to the set. For a correspondence $(y, x) \in \mathcal{N} \times \mathcal{M}$ the distortion as the mean of its deviation of relative distance to all other points in the set. Given a set of correspondences $P = p_i = (y_i, x_i) \in \mathcal{N} \times \mathcal{M}$ the distortion is defined by

the equation

$$D(p_i) = \frac{1}{|P|-1} \sum_{j \neq i} \rho(p_i, p_j) \quad (11)$$

where ρ is the individual relative distortion induced by 2 correspondences

$$\rho(p_i, p_j) = \max\left(\frac{d(y_i, y_j)}{d(x_i, x_j)}, \frac{d(x_i, x_j)}{d(y_i, y_j)}\right) \quad (12)$$

where d is the geodesic distance between 2 points. We first filter out outliers by thresholding matches whose distortion is larger than 1.2 of the mean distortion, and then greedily add from the set of DDIS maximas the point which minimizes this distortion.

5.5. Densification

If necessary, the sparse correspondences produced by our algorithm can then be passed as an input for the method of [16] to produce dense matches. This is done in a manner identical to the refinement step which is already used in the method, and improves its results.

6. implementation

Our code which produces the sparse correspondences is implemented entirely in C++ using the Point Cloud Library. For geodesics we have used Fast Marching Geodesics adapted from the code published by Ron Kimmel to run in parallel on multiple cores and in conjunction with PCL.

7. Experiments and results

In this section we will briefly go over the experiments performed and their results. We'll introduce the datasets, detail our experiments and their results

7.1. Experimental Results

In this section we will briefly go over the available Datasets **SHREC 2016 Partial Correspondence** The SHREC partial matching dataset[8] consists of 8 base, neutral pose models: cat, centaur, dog, horse, wolf, and 3 humans – 2 males, and 1 female, each containing 10,000 vertices except for the wolf which contains only 4,500 vertices. Each basic model has corresponding deformed partial shapes obtained either by cutting the shape with a plane or by adding holes on a deformed shape. The set has been divided into train and test sets. The train set is composed of 15 cuts for each base models totaling 120 models, and 10 holed shapes for each model for which ground truth point to polygon correspondences has been provided in barycentric coordinates. The test set is composed of additional 200 cuts and 200 holed shapes. We have tuned our parameters only on the 120 pairs of cuts.

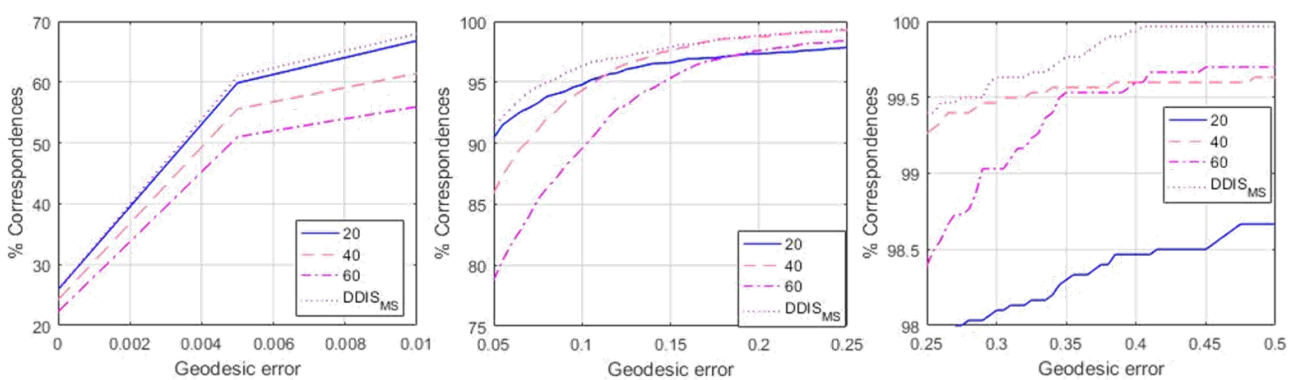


Figure 5. Effect of the β parameter on the results: it can be seen that a smaller beta promotes better localization in a small neighborhood, while higher values of β lead to more local errors but are more robust to global errors. It can be seen that the multi-scale cascade achieves better results both locally and globally.

7.2. Error Metrics

The output of partial matching algorithms (as defined in[8]) are sub-vertex point-to-point correspondences between partial shapes. For all experiments we use the standard practice of not penalizing symmetric solutions. Quality is measured according to the Princeton benchmark protocol [13]. For a pair of points $(x, y) \in \mathcal{N} \times \mathcal{M}$ between the full object \mathcal{M} and the partial shape \mathcal{N} produced by an algorithm, where (x, y^*) is the ground truth correspondence the inaccuracy is measured by. We plot curves showing the fraction of correspondences whose errors are below a threshold of the normalized geodesic error

$$\varepsilon(x) = \frac{d_{\mathcal{M}}(y, y^*)}{\sqrt{\text{area}(\mathcal{M})}} \quad (13)$$

where $d_{\mathcal{M}}(y, y^*)$ is the geodesic distance on \mathcal{M} , and has units of normalized length on \mathcal{M} . For dense correspondences over a dataset, $\varepsilon(x)$ is averaged over all matching instances.

7.2.1 Central Points Localization

In this experiment we have chosen for each Template mesh the center point c_T and tried to match it to a point on the object using DDIS. Experiments have been done using FPFH, PFH and SHOT as patch descriptors with patch radiiuses of [2, 3, 4, 5], the results of the opimal parameter for each descriptor are illustrated in fig. and visualizations of similarity maps of cuts are provided in fig. . It can be seen that good localization is obtained for points on a smooth surface, under high partiality conditions and strong deformations. Bad matches occur when a matched point resides on a heavily deformed patch, and when salient anchor points are deformed or cut. Analysis of these results shows a drift in localization occurs when salient features are divided by

strong unisometric deformations which serve as the motivation for the multiple template matching framework.

7.3. Sparse Correspondences on the SHREC16 Test set

In this experiment we have tested the performance of DDIS in producing sparse correspondences on the SHREC16 Partial Matching of Deformable Shapes competition. We had tuned our parameters on the SHREC16 training dataset using only the cuts part of it. The best results had been produced using FPFH with $r_F = 0.03\sqrt{\text{Area}(\mathcal{M})}$, and a piece size radii of $R_T = [0.6, 0.4, 0.2]\sqrt{\text{Area}(\mathcal{M})}$. For Geodesic distances we have found the fast marching algorithm to work the fastest, while giving the lowest error w.r.t. to exact geodesics. For a 10,000 vertices mesh it takes 60s to produce a full distance matrix, Though it should be noted this algorithm has a more efficient GPU implementation, and parallelization on a core brought the run time to 12s with 6 threads. FPFH and Nearest Neighbor field takes 2s, and similarity between 2 pieces of 10000 vertices each takes XXs on average, running on 6 threads of i7-2700k. Unlike optimization based algorithms this is highly parallelizable. We achieve results comparable to the state of the art [16] quality wise, even though sparser in nature on both the Cuts and the Holes datasets, Where a particularly impressive result is reported on the Holes dataset, which can then be expanded without a loss of quality by feeding these to the FSPM[16] as input instead of low level shape descriptors.

	PFM	RF	IM	EN	GT	DDIS
cuts	dense	dense	61.3	87.8	51.0	132.2
holes	dense	dense	78.2	112.6	76.4	77.3

Table 1. mean number of correspondence obtained by the algorithms in the SHREC 16 competition and our algorithm. Note that our algorithm can combine wi

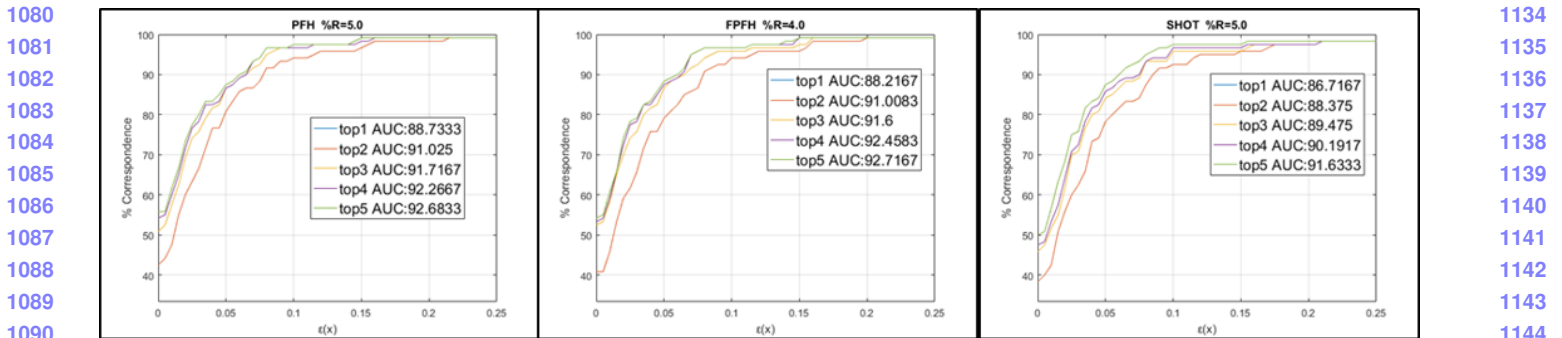


Figure 6. Comparison between descriptors: we show curves for the minimal distance of the top results. a noticeable addition occurs when adding the 2nd best match

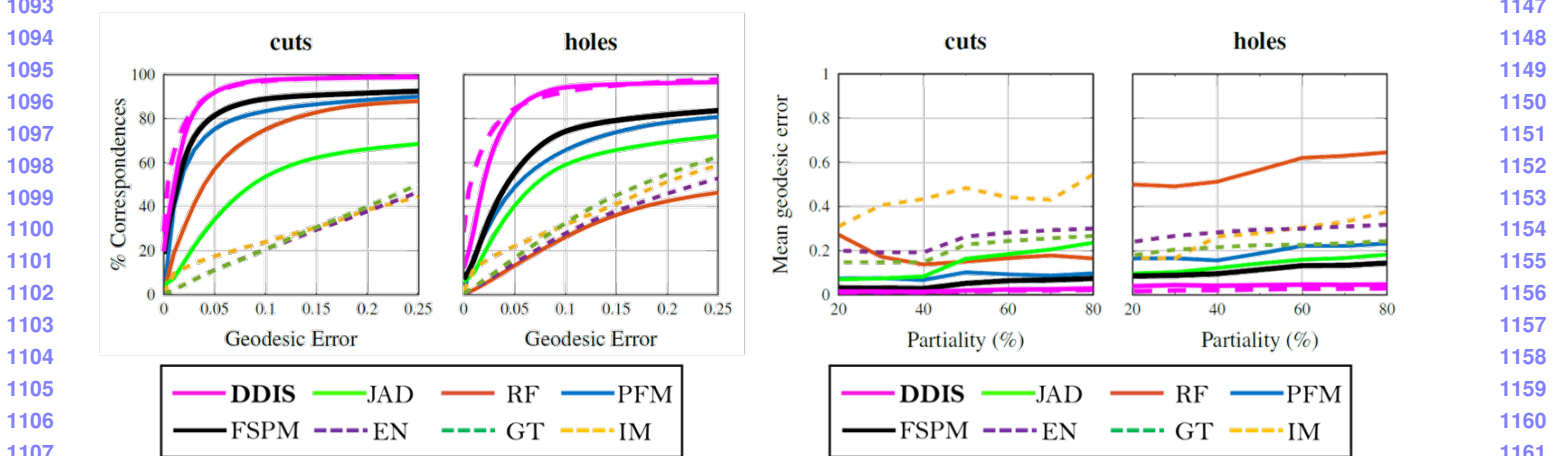


Figure 7. comparison with other state of the art algorithms - it can be seen that although sparse in nature, the correspondence obtained by DDIS are much more accurate than the other methods. A separate analysis has been done for correspondences which include boundary points, which tend to be more noisy, and internal points which are more sparse

References

- [1] D. Aiger, N. J. Mitra, and D. Cohen-Or. 4pointss congruent sets for robust pairwise surface registration. *ACM Trans. Graph.*, 27(3):85:1–85:10, Aug. 2008. 2
- [2] M. Aubry, U. Schlickewei, and D. Cremers. The wave kernel signature: A quantum mechanical approach to shape analysis. In *Computer Vision Workshops (ICCV Workshops), 2011 IEEE International Conference on*, pages 1626–1633. IEEE, 2011. 2
- [3] D. Boscaini, J. Masci, E. Rodolà, and M. Bronstein. Learning shape correspondence with anisotropic convolutional neural networks. In *Advances in Neural Information Processing Systems*, pages 3189–3197, 2016. 2
- [4] A. M. Bronstein and M. M. Bronstein. Not only size matters: regularized partial matching of nonrigid shapes. In *Computer Vision and Pattern Recognition Workshops, 2008. CVPRW’08. IEEE Computer Society Conference on*, pages 1–6. IEEE, 2008. 1, 2
- [5] A. M. Bronstein, M. M. Bronstein, A. M. Bruckstein, and R. Kimmel. Partial similarity of objects, or how to compare a centaur to a horse. *International Journal of Computer Vision*, 84(2):163, 2009. 2
- [6] A. M. Bronstein, M. M. Bronstein, and R. Kimmel. Generalized multidimensional scaling: a framework for isometry-invariant partial surface matching. *Proceedings of the National Academy of Sciences*, 103(5):1168–1172, 2006. 1, 2
- [7] M. M. Bronstein and I. Kokkinos. Scale-invariant heat kernel signatures for non-rigid shape recognition. In *Computer Vision and Pattern Recognition (CVPR), 2010 IEEE Conference on*, pages 1704–1711. IEEE, 2010. 2, 8
- [8] L. Cosmo, E. Rodolà, M. Bronstein, A. Torsello, D. Cremers, and Y. Sahillioglu. Shrec’16: Partial matching of deformable shapes. *Proc. 3DOR*, 2, 2016. 2, 9, 10
- [9] T. Dekel, S. Oron, M. Rubinstein, S. Avidan, and W. T. Freeman. Best-buddies similarity for robust template matching. In *Proceedings of the IEEE Conference on Computer Vision and Pattern Recognition*, pages 2021–2029, 2015. 3
- [10] Y. Guo, F. Sohel, M. Bennamoun, M. Lu, and J. Wan. Rotational projection statistics for 3d local surface description and object recognition. *International journal of computer vision*, 105(1):63–86, 2013. 8
- [11] D. Holz, A. E. Ichim, F. Tombari, R. B. Rusu, and S. Behnke. Registration with the point cloud library: A modular framework for aligning in 3-d. *IEEE Robotics & Automation Magazine*, 22(4):110–124, 2015. 1

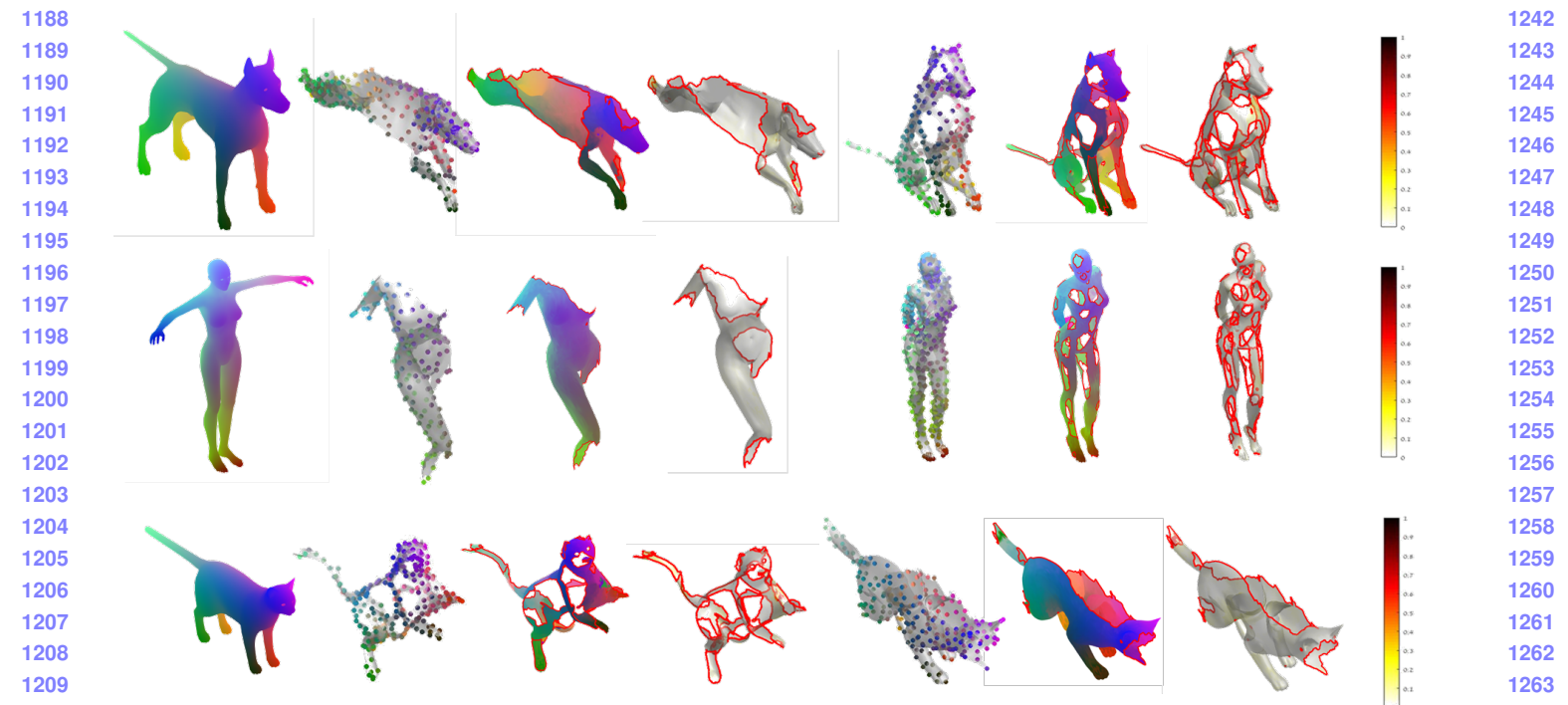


Figure 8. Good correspondences obtained by our method



Figure 9. Some notable failure cases

- [12] S. Katz, G. Leifman, and A. Tal. Mesh segmentation using feature point and core extraction. *The Visual Computer*, 21(8-10):649–658, 2005. 4, 8

[13] V. G. Kim, Y. Lipman, and T. Funkhouser. Blended intrinsic maps. In *ACM Transactions on Graphics (TOG)*, volume 30, page 79. ACM, 2011. 10

[14] A. Kovnatsky, M. M. Bronstein, X. Bresson, and P. Vandergheynst. Functional correspondence by matrix completion. In *Proceedings of the IEEE conference on computer vision and pattern recognition*, pages 905–914, 2015. 2

- 1296 [15] Y. Lipman and T. Funkhouser. Möbius voting for surface
1297 correspondence. *ACM Transactions on Graphics (TOG)*,
1298 28(3):72, 2009. 2
- 1299 [16] O. Litany, E. Rodolà, A. M. Bronstein, and M. M. Bronstein.
1300 Fully spectral partial shape matching. In *Computer Graphics
1301 Forum*, volume 36, pages 247–258. Wiley Online Library,
1302 2017. 1, 2, 9, 10
- 1303 [17] J. Masci, E. Rodolà, D. Boscaini, M. M. Bronstein, and
1304 H. Li. Geometric deep learning. In *SIGGRAPH ASIA 2016
1305 Courses*, page 1. ACM, 2016. 2
- 1306 [18] N. Max. Weights for computing vertex normals from facet
1307 normals. *Journal of Graphics Tools*, 4(2):1–6, 1999. 6
- 1308 [19] F. Monti, D. Boscaini, and J. Masci. Geometric deep learning
1309 on graphs and manifolds using mixture model cnns. 2
- 1310 [20] M. Ovsjanikov, M. Ben-Chen, J. Solomon, A. Butscher, and
1311 L. Guibas. Functional maps: A flexible representation of
1312 maps between shapes. *ACM Trans. Graph.*, 31(4):30:1–
1313 30:11, July 2012. 1, 2
- 1314 [21] J. Pokrass, A. M. Bronstein, and M. M. Bronstein. Partial
1315 shape matching without point-wise correspondence. *Numerical
1316 Mathematics: Theory, Methods and Applications*,
1317 6(1):223–244, 2013. 2
- 1318 [22] J. Pokrass, A. M. Bronstein, M. M. Bronstein, P. Sprech-
1319 mann, and G. Sapiro. Sparse modeling of intrinsic cor-
1320 respondences. In *Computer Graphics Forum*, volume 32,
1321 pages 459–468. Wiley Online Library, 2013. 2
- 1322 [23] E. Rodolà, S. R. Bulò, T. Windheuser, M. Vestner, and
1323 D. Cremers. Dense non-rigid shape correspondence using
1324 random forests. In *Proceedings of the 2014 IEEE Confer-
1325 ence on Computer Vision and Pattern Recognition, CVPR
1326 '14*, pages 4177–4184, Washington, DC, USA, 2014. IEEE
1327 Computer Society. 2
- 1328 [24] E. Rodolà, L. Cosmo, M. M. Bronstein, A. Torsello, and
1329 D. Cremers. Partial functional correspondence. In *Computer
1330 Graphics Forum*, volume 36, pages 222–236. Wiley Online
1331 Library, 2017. 1, 2
- 1332 [25] E. Rodola, A. Torsello, T. Harada, Y. Kuniyoshi, and D. Cre-
1333 mers. Elastic net constraints for shape matching. In *Pro-
1334 ceedings of the IEEE International Conference on Computer
1335 Vision*, pages 1169–1176, 2013. 2
- 1336 [26] R. B. Rusu, N. Blodow, and M. Beetz. Fast point feature
1337 histograms (fpfh) for 3d registration. In *Robotics and Au-
1338 tonation, 2009. ICRA'09. IEEE International Conference
1339 on*, pages 3212–3217. Citeseer, 2009. 1, 2, 3, 6, 8
- 1340 [27] R. B. Rusu, Z. C. Marton, N. Blodow, and M. Beetz. Learn-
1341 ing informative point classes for the acquisition of object
1342 model maps. In *Control, Automation, Robotics and Vi-
1343 sion, 2008. ICARCV 2008. 10th International Conference
1344 on*, pages 643–650. IEEE, 2008. 2, 8
- 1345 [28] R. B. Rusu, Z. C. Marton, N. Blodow, M. Dolha, and
1346 M. Beetz. Towards 3d point cloud based object maps for
1347 household environments. *Robotics and Autonomous Sys-
1348 tems*, 56(11):927–941, 2008. 2, 3
- 1349 [29] Y. Sahillioğlu and Y. Yemez. Minimum-distortion iso-
1350 metric shape correspondence using em algorithm. *IEEE
1351 transactions on pattern analysis and machine intelligence*,
1352 34(11):2203–2215, 2012. 2, 8, 9
- 1353 [30] Y. Sahillioğlu and Y. Yemez. Scale normalization for iso-
1354 metric shape matching. In *Computer Graphics Forum*, vol-
1355 ume 31, pages 2233–2240. Wiley Online Library, 2012. 2
- 1356 [31] Y. Sahillioğlu and Y. Yemez. Coarse-to-fine combinatorial
1357 matching for dense isometric shape correspondence. In *Com-
1358 puter Graphics Forum*, volume 30, pages 1461–1470. Wiley
1359 Online Library, 2011. 2, 8, 9
- 1360 [32] A. Shtern and R. Kimmel. Matching the lbo eigenspace of
1361 non-rigid shapes via high order statistics. *Axioms*, 3(3):300–
1362 319, 2014. 2
- 1363 [33] J. Sun, M. Ovsjanikov, and L. Guibas. A concise and prov-
1364 ably informative multi-scale signature based on heat diffu-
1365 sion. In *Proceedings of the Symposium on Geometry Pro-
1366 cessing, SGP '09*, pages 1383–1392, Aire-la-Ville, Switzer-
1367 land, Switzerland, 2009. Eurographics Association. 3, 8
- 1368 [34] I. Talmi, R. Mechrez, and L. Zelnik-Manor. Template match-
1369 ing with deformable diversity similarity. In *Proc. of IEEE
1370 Conf. on Computer Vision and Pattern Recognition*, pages
1371 1311–1319, 2017. 1, 3, 5, 8
- 1372 [35] F. Tombari, S. Salti, and L. Di Stefano. Unique signatures of
1373 histograms for local surface description. In *European con-
1374 ference on computer vision*, pages 356–369. Springer, 2010.
1375 2, 3, 8
- 1376 [36] A. Torsello. A game-theoretic approach to deformable shape
1377 matching. In *Proceedings of the 2012 IEEE Conference on
1378 Computer Vision and Pattern Recognition (CVPR), CVPR
1379 '12*, pages 182–189, Washington, DC, USA, 2012. IEEE
1380 Computer Society. 1, 2
- 1381 [37] M. Vestner, Z. Lähner, A. Boyarski, O. Litany, R. Slossberg,
1382 T. Remez, E. Rodola, A. Bronstein, M. Bronstein, R. Kim-
1383 mel, et al. Efficient deformable shape correspondence via
1384 kernel matching. In *3D Vision (3DV), 2017 International
1385 Conference on*, pages 517–526. IEEE, 2017. 1, 2
- 1386 [38] M. Vestner, Z. Lähner, A. Boyarski, O. Litany, R. Slossberg,
1387 T. Remez, E. Rodola, A. Bronstein, M. Bronstein, R. Kim-
1388 mel, et al. Efficient deformable shape correspondence via
1389 kernel matching. In *3D Vision (3DV), 2017 International
1390 Conference on*, pages 517–526. IEEE, 2017. 1, 2
- 1391 [39] M. Vestner, Z. Lähner, A. Boyarski, O. Litany, R. Slossberg,
1392 T. Remez, E. Rodola, A. Bronstein, M. Bronstein, R. Kim-
1393 mel, et al. Efficient deformable shape correspondence via
1394 kernel matching. In *3D Vision (3DV), 2017 International
1395 Conference on*, pages 517–526. IEEE, 2017. 1, 2
- 1396 [40] M. Vestner, Z. Lähner, A. Boyarski, O. Litany, R. Slossberg,
1397 T. Remez, E. Rodola, A. Bronstein, M. Bronstein, R. Kim-
1398 mel, et al. Efficient deformable shape correspondence via
1399 kernel matching. In *3D Vision (3DV), 2017 International
1400 Conference on*, pages 517–526. IEEE, 2017. 1, 2
- 1401 [41] M. Vestner, Z. Lähner, A. Boyarski, O. Litany, R. Slossberg,
1402 T. Remez, E. Rodola, A. Bronstein, M. Bronstein, R. Kim-
1403 mel, et al. Efficient deformable shape correspondence via
1404 kernel matching. In *3D Vision (3DV), 2017 International
1405 Conference on*, pages 517–526. IEEE, 2017. 1, 2